Exceptional points in single open acoustic resonator due to symmetry breaking

Vladimir Igoshin [1], Mariia Tsimokha,[1] Anastasia Nikitina [1], Mihail Petrov [1,*], Ivan Toftul [1], and Kristina Frizyuk [1,2,†]
[1]*The School of Physics and Engineering, ITMO University, 197101 Saint Petersburg, Russia*
[2]*Department of Information Engineering, University of Brescia, Via Branze 38, 25123 Brescia, Italy*

(Received 4 July 2023; revised 17 February 2024; accepted 12 March 2024; published 4 April 2024)

Exceptional points (EPs) have been widely studied in quantum mechanics, condensed-matter physics, optics, and photonics. However, their potential in acoustics has only recently been recognized due to the rapid development of acoustic metamaterials. This paper proposes a method for achieving EP conditions in acoustic resonators by lowering their symmetry and enabling resonant-mode interaction. The formation of EPs is predicted through direct numerical simulation supported by coupled-mode theory and resonant state expansion. These findings have significant implications for the design and optimization of acoustic metamaterials for applications such as acoustic sensing and noise reduction.

DOI: 10.1103/PhysRevB.109.144102

I. INTRODUCTION

Acoustic metamaterials are a promising class of materials that offer unique capabilities for tailoring properties of sound waves [1–3] as well as for mechanical manipulation [4–6]. While resonances play a central role in acoustic metamaterials, there are still many unexplored physical effects and mechanisms. Exceptional points (EPs) are the points in the parameter space where the eigenvalues of the system become degenerate and the eigenvectors coalesce, leading to a nondiagonalizable Jordan block formation [7–10]. The EP systems' states are excellent candidates for sensing applications since their spectral singularities are highly responsive to external parameter changes or any perturbations [11,12]. Despite the progress in this area, the problem of EP appearance in single acoustic resonators still requires thorough study, and it is addressed in this paper.

EPs occur only in non-Hermitian systems [10], and they are often mentioned in the context of $\mathcal{PT}$-symmetric systems [8,13–17] observed in electronics [18], optics, and photonics [11,13,15], and recently in acoustics [19,20]. However, reaching $\mathcal{PT}$-symmetry requires particular engineering of gain and loss in acoustical systems. Alternatively, EPs can be observed in open resonators as a special class of non-Hermitian systems which was extensively studied in optics and photonics [15,21,22]. One of the possible mechanisms of EP formation is based on *breaking the symmetry of the resonator* [23,24]. While this is not a unique approach, we leave the other methods beyond the scope of the current work and refer the readers to Refs. [8,25]. However, despite extensive research on EPs in optics, there has been little work on EPs in the acoustics domain.

In this work, we show that by engineering the shape of resonators and due to related symmetry breaking, one can enable mode-coupling mechanisms leading to the formation of the EP condition as schematically shown in Fig. 1: in a system with perturbed symmetry, two initially noninteracting modes transform into two different modes via a degenerate state. This transitional state appears to be an EP state.

We improve and adapt the powerful method of multipolar analysis [26–28] to (i) predict the occurrence of EPs as a result of a particular symmetry breaking and (ii) to understand the mode interaction deeper within a coupled-mode theory and resonant state expansion (RSE) method.

Exploring the physics behind the EPs' formation in acoustic resonators may unlock novel methods for the design and optimization of acoustic metamaterials for a wide range of applications, such as sound focusing [29], optomechanics [30], sensing [31–34], noise insulation [35], and seismic cloaking [36,37]. By addressing the important questions surrounding the physics of acoustic metamaterials, we may open the door to new and exciting opportunities in acoustics and materials science.

This work is organized as follows. In Sec. II we build a simple model based on the linear acoustic equations and discuss the simple mechanism of the EP appearance. In Sec. III we extend the approach to more complex symmetries and generalize the method. Finally, in Sec. IV we conclude the obtained results.

II. COUPLING OF MODES IN ACOUSTIC RESONATORS

A. Model physics and parameters

We focus on the studies of resonators in the framework of linear acoustics in the frequency domain. The resonator is made of homogeneous acoustic materials and placed in a homogeneous environment (fluid or gas), which supports only longitudinal waves (Fig. 1). The media and the resonator are both characterized by their compressibility β and their mass density ρ. The speed of sound is given by $c = 1/\sqrt{\beta\rho}$. The complex velocity $\mathbf{v}(\mathbf{r})$ and pressure $p(\mathbf{r})$ fields satisfy

*m.petrov@metalab.ifmo.ru
†k.frizyuk@metalab.ifmo.ru

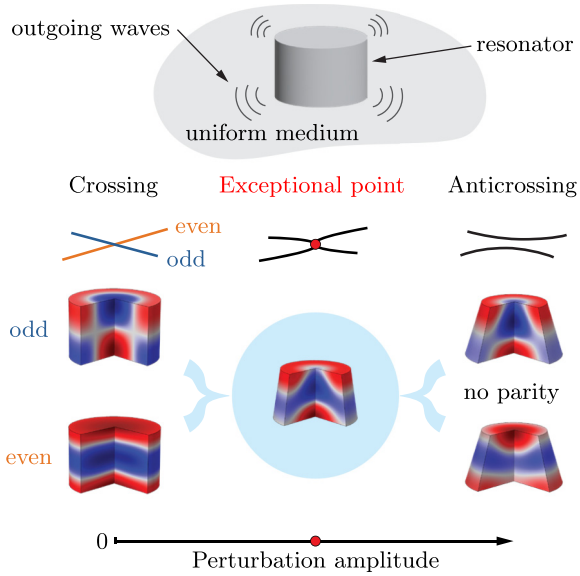

FIG. 1. The main idea and setup of this work. Symmetry-breaking perturbation merges two groups of resonator's modes induced by symmetry considerations into a single group. This is shown at the bottom of the figure. By changing the amplitude of the symmetry-breaking perturbation, we can tune the coupling strength. As shown in the middle of the figure, this allows us to observe the transition from the crossing of energy terms to avoided crossing. This transition can be followed by an EP, characterized by the coalescence of eigenspaces.

the wave equations; if the harmonic convention $\exp(-i\omega t)$ is assumed [38],

$$i\omega\beta p = \nabla\cdot\mathbf{v}, \quad i\omega\rho\mathbf{v} = \nabla p. \tag{1}$$

This can be written in a matrix form as

$$\underbrace{\begin{pmatrix} 0 & -\nabla\cdot \\ \nabla & 0 \end{pmatrix}}_{\hat{\mathbb{D}}} \underbrace{\begin{pmatrix} p \\ i\mathbf{v} \end{pmatrix}}_{\vec{\mathbb{F}}} = \omega \underbrace{\begin{pmatrix} \beta(\mathbf{r}) & 0 \\ 0 & \rho(\mathbf{r}) \end{pmatrix}}_{\hat{\mathbb{P}}} \underbrace{\begin{pmatrix} p \\ i\mathbf{v} \end{pmatrix}}_{\vec{\mathbb{F}}}, \tag{2}$$

which describes the eigenmodes $\vec{\mathbb{F}}(\mathbf{r})$ of an open acoustic resonator, where the operators $\hat{\mathbb{D}}(\mathbf{r})$ and $\hat{\mathbb{P}}(\mathbf{r})$ are introduced for future convenience.

The boundary conditions play a crucial role in determining the symmetry of the system. The system's symmetry is determined not only by the shape of the resonator boundary but also by the conditions imposed on these boundaries. In this work, the symmetry of the boundary conditions is identical to the symmetry of the resonator. The boundary conditions at the particle-host interface require continuity of pressure $p(\mathbf{r})$ and the normal component of velocity $\mathbf{v}(\mathbf{r})$ [38]. At $|\mathbf{r}| \to +\infty$, the Sommerfeld radiation condition applies, ensuring the existence of only physically meaningful radiating eigenmodes [39,40]. This condition exhibits spherical symmetry because it only depends on $|\mathbf{r}|$. As any point group and limiting point group represent subgroups of the symmetry group of the sphere [41,42], this condition does not affect the system's symmetry group defined by the resonator's shape and boundary conditions at the particle-host interface. Also, introduction of dissipation via, for example, viscosity will keep the symmetry of the problem, and all the main conclusions of our work will remain valid.

The formulated eigenvalue problem is in a full analogy to the one appearing in optics [43,44]. Eigenmodes of this system can be classified by irreducible representations (irreps) of a symmetry group of a resonator [26,45,46] similarly to the case of optical resonators [27]. Some particular material parameters have been chosen to illustrate the general conclusions of this paper which, in general, do not depend on this choice. Although resonators made of high-contrast materials are much easier to observe resonances in, the resonant states can be studied in various systems [47,48]. For most acoustic experiments performed in air, the wavelength in the resonator is longer than that in the host medium. However, we have chosen our parameters in favor of numerical stability since all conclusions do not depend on whether the acoustic refractive index c_0/c_1 is greater or less than 1. To be specific, we use the density $\rho_0 = 1\ \mathrm{kg/m^3}$ and the speed of sound $c_0 = 1\ \mathrm{m/s}$ for the media and $\rho_1 = \rho_0/2$ and $c_1 = c_0/2$ for the resonator; therefore, the refractive index is greater than 1.

It is also worth noting that a similar scenario is also possible in practice: Mie-resonant acoustic meta-atoms can be used to create metamaterials with a high effective refractive index [5,49–51]. Nevertheless, we stress again that the theory presented below does not depend on the material parameters of the media and the resonator as soon as the system supports resonant modes.

The computations of eigenmodes were performed with help of numerical simulations in COMSOL MULTIPHYSICS and the method is described in Appendix D.

B. EP appearance

To clarify the connection between symmetry and EP formation, we first elaborate on the resonator spectrum modification with the change of the resonator shape. Starting with highly symmetric structures like cylinders [26], we move to more complex shapes later. We fix the initial geometry of the cylinder such that the height-to-radius ratio is $h_0/R_0 = 2$ [see Fig. 3 (inset)].

The cylinder corresponds to the $D_{\infty h}$ symmetry group; thus, it has a countably infinite set of finite-dimensional irreducible representations [52–54]. In Fig. 2 each representation is shown alongside corresponding examples of numerically calculated pressure fields. Each of those irreducible representations of a symmetry group of a cylinder corresponds to a single value of the azimuthal number m. In the following, we narrow the consideration to $m = 0$ only, or, in more specific terms, eigenmodes that transformed under irreducible representations A_{1u} and A_{1g}. These eigenmodes exhibit rotational symmetry but have different parity under horizontal reflection (σ_h transformation). The obtained results can be straightforwardly extended to other azimuthal numbers m. We exclude the monopole mode which transforms under the irreducible representation A_{1g} in favor of another more illustrative example. However, we emphasize that during the symmetry breaking $D_{\infty h} \to C_{\infty v}$ (e.g., cylinder to cone), monopole and dipole modes start to transform under the same irreducible representation A_1 in the cone symmetry group and hence interact with each other. The scatterers which exhibit interaction

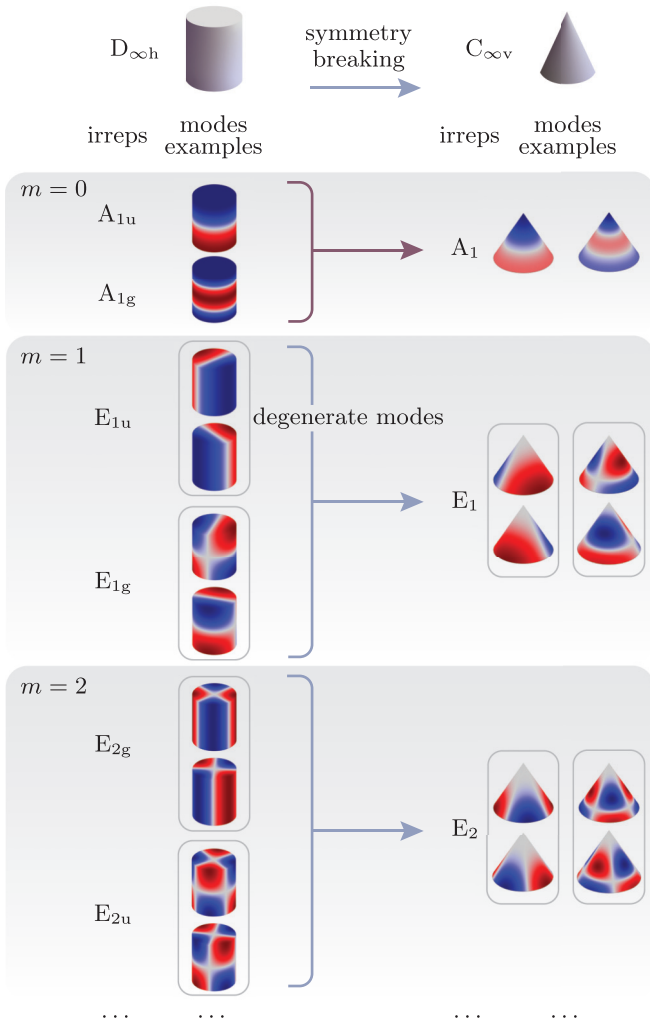

FIG. 2. Tables of irreducible representations of symmetry groups $D_{\infty h}$ and $C_{\infty v}$ and examples of the eigenmodes which transform under these irreps. Only the first few irreps are shown. Examples of modes that transform under the particular irreducible representations are given. The monopole mode transforms under the irreducible representation A_{1g} but is omitted in the figure in favor of a more illustrative mode. The arrows show how the irreducible representations of the two groups are related to each other.

between the monopole and dipole moments are conventionally characterized by Willis coupling [6,55–57]. This requires the absence of the inversion symmetry and that the monopole and the dipole are transformed by the same irreducible representation.

The dependence of the real part of the eigenfrequency of the $m = 0$ modes on the resonator's height is shown in Fig. 3(b). The wave vector k is related to the eigenfrequency ω as follows: $k = \omega/c_1$. Each color of the line represents a different irreducible representation, either A_{1u} or A_{1g}. Hereafter, we denote eigenmodes transformed under irreducible representations A_{1u} and A_{1g} as mode A_{1u} and mode A_{1g}, respectively. At this point, it should be mentioned that modes transforming under different irreps are orthogonal; therefore, coupling between them does not occur [45,46]. In Fig. 3(b), this statement can be interpreted visually, where the crossing

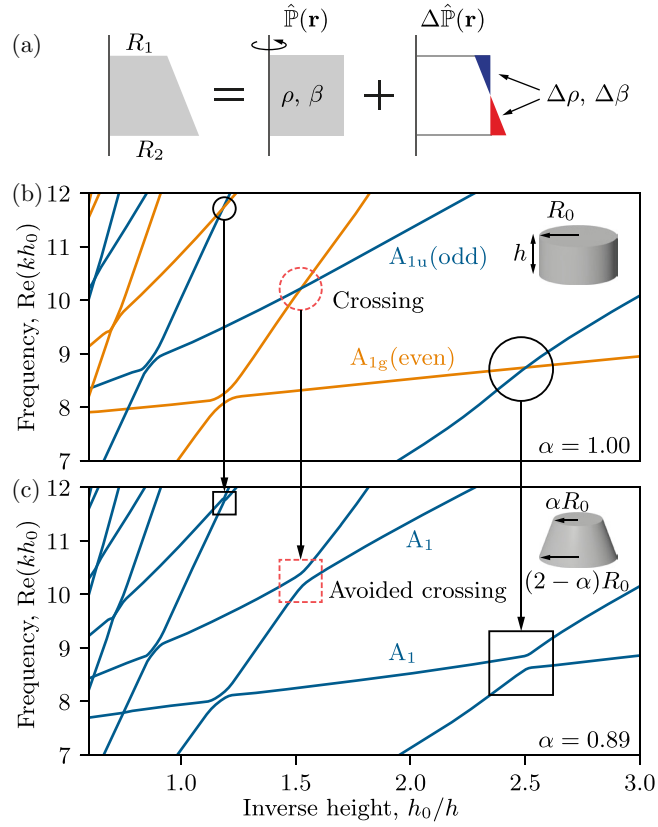

FIG. 3. (a) Geometry of the system and shape perturbation. Real parts of eigenvalues k scaled to h_0 of a cylinder with $\alpha = 1$ (b) and a conical frustum with $\alpha = 0.89$ (c) versus h_0/h. The branches of the cylinder's modes have different colors according to their irreps. Intersections of modes that transform under different irreps are circled. Corresponding avoided crossings and crossing with weak coupling are marked with a square. The crossing and the avoided crossing shown in Fig. 4 are dashed. Geometry parameters used are $h_0 = 1$ m and $R_0 = 0.5$ m.

between two orthogonal modes of a cylinder, A_{1u} and A_{1g}, occurs. Indeed, explicit analysis of the eigenmodes' fields shows that these modes have different parities, "odd" and "even" correspondingly, with respect to σ_h (reflection in the horizontal plane) transformation. In contrast, Fig. 3(b) shows the avoided crossing behavior of the eigenfrequency lines of the modes related to the same irrep.

Next, one can alter the symmetry of the resonator by perturbing its shape from cylinder to cone, breaking the mirror symmetry in the horizontal plane. In order to carefully trace out changes in the mode structure, those changes should be made gradually. We define the parameter of "cylindricity" of the resonator's shape α [Fig. 3(c)], which denotes the amplitude of the shape perturbation. In terms of α, the resonator's upper base radius R_1 and lower base radius R_2 [Fig. 3(a)] can be expressed as follows:

$$R_1 = \alpha R_0 = R_0 + (\alpha - 1)R_0, \tag{3}$$

$$R_2 = R_0 + (1 - \alpha)R_0. \tag{4}$$

Varying α from 1 to 0 reduces the upper base radius of the cylinder, while simultaneously increasing the lower base

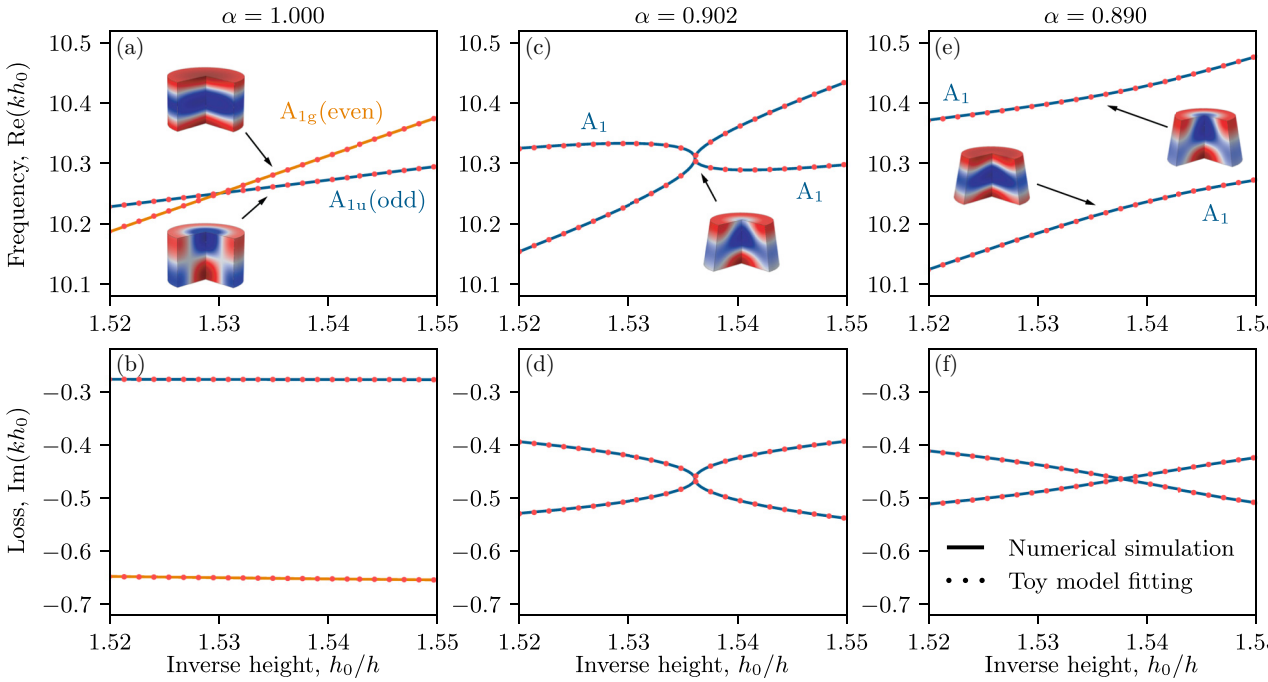

FIG. 4. Maps of real and imaginary parts of eigenvalues k of the acoustic resonator (scaled to h_0). Examples of fields in resonators are given. (a) The crossing of real parts of two noninteracting modes that transform under different irreps A_{1u} and A_{1g} is observed at "cylindricity" parameter $\alpha = 1.000$. (e) At $\alpha = 0.890$ there is an anticrossing of real parts of modes that transform under the same irrep A_1 (strong coupling). At $\alpha = 0.902$ an EP is achieved in which both real (c) and imaginary (d) parts of eigenvalues are crossed, and therefore modes degenerate. A toy model fitting is discussed in Appendix C.

radius. Thus, decreasing the parameter α breaks the symmetry with respect to σ_h and changes the symmetry group of the system from $D_{\infty h}$ to $C_{\infty v}$. As shown in Fig. 2, the previously considered A_{1u} and A_{1g} modes lose their specific σ_h parity property and now transform under the same irrep A_1. Therefore, a coupling between those modes should now appear in conical symmetry which manifests itself in the appearance of avoided crossings between the frequency lines shown in Fig. 3(c). The transition from crossing to avoided crossing induced by symmetry breaking is shown with arrows.

To this point, almost exclusively the real part of the eigenfrequency was discussed. Imaginary parts of the eigenfrequencies are shown in Fig. 4(b). While a crossing behavior in real parts [Fig. 4(a)] can be observed, imaginary parts are not equal, and the modes are not degenerate. However, by varying the height of the resonator h and the cylindricity parameter α, at a certain coupling strength, the simultaneous degeneracy of real and imaginary parts of two modes is observed [see Figs. 4(c) and 4(d)].

Now the series of Figs. 4(a), 4(c), and 4(e) can be regarded as follows: from left to right three different stages of the resonator's deformation from a cylinder to a cone are shown. At the most left [Figs. 4(a) and 4(b)], a $D_{\infty h}$ symmetry of the resonator ensures a complete absence of any interaction between the two considered modes; at the most right [Figs. 4(e) and 4(f)] the interaction is great enough to keep those modes entirely apart from each other; evidently, based on the smoothness of this particular symmetry breaking, at the intermediate parameters shown in Figs. 4(c) and 4(d), a point corresponding to full degeneracy of two modes can be found. In Figs. 4(c) and 4(d) two lines merge into a single point, both for the real and imaginary parts of the frequency, which corresponds to the formation of the EP. Note, that the usual degeneracy of two modes happens in so-called diabolic points [10], which correspond to the two- or more-dimensional irreps. However, in this case, the fact that the A_1 irrep is one-dimensional makes this not even possible. In simple words, we cannot obtain two A_1 modes with the same frequency whose fields are linearly independent [11,13,25,58].

One should also note that the crossing-to-avoided-crossing mechanism is precisely inverted for real and imaginary parts, as shown in Figs. 4(b), 4(d), and 4(f), where the system goes from an anticrossing, through a degeneracy, to a crossing. The observed modes' interaction via symmetry breaking can be extended to other resonator shapes as discussed in Appendix B.

The symmetry of a system can be changed not only by perturbing its shape but also by perturbing its boundary conditions. In this work, we use shape perturbation as the simple and most demonstrative approach.

C. Coupled-mode theory and perturbation of the material parameters

The appearance of EP in quantum mechanics and optics can often be interpreted within the scope of a standard coupled-mode theory, described by a 2×2 Hamiltonian of a two-level system [8,11,13,25,58]. While the coupling of several acoustic resonators has already been analyzed within standard coupled-mode theory [59,60], the mode coupling in a single acoustic resonator upon its shape perturbation has not yet been discussed. In this section, we introduce the

phenomenological model of interaction of two eigenmodes based on RSE or quasinormal mode expansion [43,61–63]. RSE has already proved its efficiency for determining the eigenmodes of a perturbed optical system, the appearance of a strong-coupling regime [64], and multipole coupling [27]. We aim to provide such analysis for the linear acoustics described by Eq. (2). These equations can be rewritten in a compact form similar to that of Ref. [43]:

$$\hat{\mathbb{D}}(\mathbf{r})\vec{\mathbb{F}}_n(\mathbf{r}) = \omega_n \hat{\mathbb{P}}(\mathbf{r})\vec{\mathbb{F}}_n(\mathbf{r}), \tag{5}$$

where $\vec{\mathbb{F}}_n(\mathbf{r}) = (p_n, \quad i\mathbf{v}_n)^\intercal$ is an eigenmode and ω_n is an eigenvalue. For the perturbed resonator there is a new set of eigenmodes $\vec{\mathbb{F}}(\mathbf{r})$ and eigenvalues Ω:

$$\hat{\mathbb{D}}(\mathbf{r})\vec{\mathbb{F}}(\mathbf{r}) = \Omega(\hat{\mathbb{P}}(\mathbf{r}) + \Delta\hat{\mathbb{P}}(\mathbf{r}))\vec{\mathbb{F}}(\mathbf{r}), \tag{6}$$

where $\Delta\hat{\mathbb{P}}(\mathbf{r}) = \mathrm{diag}[\Delta\beta(\mathbf{r}), \Delta\rho(\mathbf{r})]$ represents the perturbation of density $\rho(\mathbf{r})$ and compressibility $\beta(\mathbf{r})$ spatial distributions, caused, for example, by changing the resonator's shape. The concept of $\Delta\hat{\mathbb{P}}(\mathbf{r})$ as a shape perturbation for cylinder to cone transition is illustrated in Fig. 3(a).

It is assumed that all eigenmodes are a linear combination of eigenmodes of the unperturbed system $\vec{\mathbb{F}}(\mathbf{r}) = \sum_n c_n \vec{\mathbb{F}}_n(\mathbf{r})$. Within this approach, the perturbation theory formalism [43] immediately provides us with the coupled-equations system

$$\sum_n [(\Omega - \omega_n)\delta_{mn} + \Omega V_{mn}]c_n = 0, \tag{7}$$

where $V_{mn} \propto \int \vec{\mathbb{F}}_m^\intercal \Delta\hat{\mathbb{P}}\vec{\mathbb{F}}_n \mathrm{d}^3\mathbf{r}$ is the matrix element. The integral is taken over the region where the perturbation is nonzero. In the case of the cylinder perturbation to a cut cone, the integration space can be achieved by subtracting the cylinder from a cut cone [Fig. 3(a)]. In the two-mode approximation of Eq. (7), we obtain the eigenvalue problem

$$\begin{pmatrix} \omega_1 & 0 \\ 0 & \omega_2 \end{pmatrix}\begin{pmatrix} c_1 \\ c_2 \end{pmatrix} = \Omega\begin{pmatrix} 1+V_{11} & V_{12} \\ V_{12} & 1+V_{22} \end{pmatrix}\begin{pmatrix} c_1 \\ c_2 \end{pmatrix}. \tag{8}$$

The eigenvalues of this equation are

$$\Omega_\pm = \frac{\xi\omega_2 + \gamma\omega_1 \pm \sqrt{(\xi\omega_2 - \gamma\omega_1)^2 + 4\kappa^2\omega_1\omega_2}}{2(\xi\gamma - \kappa^2)}, \tag{9}$$

where $\kappa = V_{12} = V_{21}$, $\xi = 1 + V_{11}$, and $\gamma = 1 + V_{22}$. It can be seen that the nondiagonal element κ is responsible for the coupling between the modes.

The main condition for observing EPs can be summarized as $\Omega_- = \Omega_+$. Or, in a more extended form, $(\xi\omega_2 - \gamma\omega_1)^2 + 4\kappa^2\omega_1\omega_2 = 0$. It can be seen that if this condition is satisfied and $\kappa \neq 0$, the eigenspaces collapse.

Here, we show that this system can be applied to describing the EP formation in acoustic resonators with symmetry breaking. Determining the exact values of governing parameters κ, ξ, and γ requires introducing the proper scalar product and normalization and remains beyond the scope of the current work. Still, we find these parameters numerically by fitting the real and imaginary frequency curves in Fig. 4 within Eq. (9) (see Appendix C for the details). The obtained results, shown as dots in Fig. 4, demonstrate excellent correspondence to the numerical results.

Within the coupled-mode approach it becomes evident that two modes that transform under the same irrep may couple to each other since the coupling constant provided by the integral $\kappa \propto \int \vec{\mathbb{F}}_1^\intercal \Delta\hat{\mathbb{P}}\vec{\mathbb{F}}_2 \mathrm{d}^3\mathbf{r} \neq 0$ in full accordance with Wigner's theorem [65]. It can also be derived from the selection rules presented in Refs. [45,46].

III. GENERALIZATION OF THE APPROACH TO OTHER SYMMETRIES

The illustrated mechanism of EP formation can be extended to resonators of arbitrary shapes. The general recipe for that is as follows.

(i) Two noninteracting eigenmodes, which transform under different irreps, have to be chosen.

(ii) Next, by particular symmetry breaking one needs to ensure that these modes will appear in the same irrep. This step is essential, as the chosen symmetry will trigger the formation of EP states.

(iii) Now the original symmetry has to be broken smoothly for transition from an object of the original symmetry to one of the chosen new symmetry; in other words, we have a homotopy (see Appendix A). Thus, the shape change is moderated by one parameter. This way, an appearance of EP can be traced easily.

Following this algorithm, one can observe EP formation in more complex shapes and symmetries of the resonator. As an example, besides the already considered $D_{\infty h}$ to $C_{\infty v}$ symmetry breaking, one can observe EP formation in C_{4v} to C_{2v} symmetry breaking as discussed in detail in Appendix B and supported by numerical simulations. Formation of the EP is provided, for example, by the merging of B_1 and A_1 irreps into A_1.

In strong contrast to $\mathcal{PT}$-symmetric systems, which are often used for achieving the EP condition, breaking point symmetry discussed in this work does not require balancing of loss and gain and, thus, is easier to achieve. At the same time, the $\mathcal{PT}$-symmetric structures offer unique effects [66] provided by their higher symmetry.

IV. CONCLUSION

In this work, a general mechanism for retrieving exceptional points in complex acoustic systems is proposed. We identify an approach to achieving the exceptional point condition by breaking a particular symmetry of the resonator, leading to the coupling of initially orthogonal eigenmodes. Smooth variation of the asymmetry parameter allows for finding the exact conditions for mode coalescence. This mechanism was illustrated in single homogeneous acoustic resonators by breaking their symmetry from $D_{\infty h}$ to $C_{\infty v}$ and from C_{4v} to C_{2v}. The results were supported by direct numerical simulations. Moreover, we proposed a phenomenological model of the interaction of two eigenmodes based on the resonant state expansion method and perturbation theory. We have verified that the proposed description in the two-mode approximation can be used for qualitative analysis of eigenfrequencies. The proposed mechanism of EP formation can be potentially realized experimentally in open resonators in the acoustic scattering regime. One of the main conditions is the existence of high-quality resonances allowing for resolving the corresponding resonant peaks' emergence and separation.

ACKNOWLEDGMENTS

The analytical calculations were supported by the Russian Science Foundation under Grant No. 20-72-10141 while the numerical simulations were supported by the Ministry of Science and Higher Education of the Russian Federation under Grant No. 075-15-2022-1120. The work was supported by the Academic Leadership Program Priority 2030. M.P. acknowledges support from the Foundation for the Advancement of Theoretical Physics and Mathematics "BASIS".

APPENDIX A: PARAMETER α

Generally, there are many ways of how the parameter α can be defined, and often, no formal definition is required for particular geometries. At the same time, we need to note that utilizing the concept of homotopy is a useful approach that requires only a single parameter α to describe any symmetry breaking, even though the explicit description of the map might be nontrivial in particular cases [67,68]. Below we introduce the description of the parameter α in these terms.

Assume that we have two maps of a topological space X into $\mathbb{R}^3$, $f, g : X \to \mathbb{R}^3$ (e.g., g and f represent cone and cylinder as maps of a 3-ball, torus and mug as maps of a solid torus, etc.).

Two maps f and g are homotopic [69] if there exists a continuous map $H : X \times [0, 1] \to \mathbb{R}^3$ from the product of the space X with the unit interval [0,1] to $\mathbb{R}^3$, $(x, \alpha) \to h_\alpha(x)$ for $x \in X$, $\alpha \in [0, 1]$ such that $h_0(x) = f(x)$ and $h_1(x) = g(x)$. Thus, we have a homotopy between the maps f and g, parametrized by α.

APPENDIX B: EXAMPLE OF $C_{4v} \to C_{2v}$ TRANSITION

The mechanism of EP formation described above is very general and is based on symmetry requirements.

Having two modes which show a crossing behavior in the unperturbed system, we break the symmetry in a way that makes these modes interact (i.e., merges two irreps into a single one, so two modes, which transform by the different irreps, will be transformed by the same irrep after the perturbation). The EP state occurrence for $D_{\infty h} \to C_{\infty v}$ symmetry breaking, which has already been considered above, can be generalized to more complex cases such as the transition $C_{4v} \to C_{2v}$.

The merging A_1 and B_1 modes of the regular square pyramid C_{4v} to A_1 modes of the rectangular right pyramid C_{2v} are shown in Fig. 5. Note that this is closely related to the correlation tables, which are widely used in solid-state physics [70–72]. Figure 6 illustrates crossing between the two orthogonal modes A_1 and B_1 of the regular square pyramid and avoided crossing between the two modes of the rectangular right pyramid that transform under same irreducible representation A_1. In this case avoided crossing and exceptional points can be easily achieved due to the symmetry breaking and the proper selection of parameters.

APPENDIX C: TOY MODEL FITTING

In order to test the ability of the model (Sec. II C) to describe the effects presented in Fig. 4, we fit its parameters ξ, γ, and κ. A range of heights h_0/h from 1.52 to 1.55 is used to illustrate the square root behavior in the vicinity of EP, model parameters are assumed to be constant over the chosen range. Eigenfrequencies for the unperturbed system

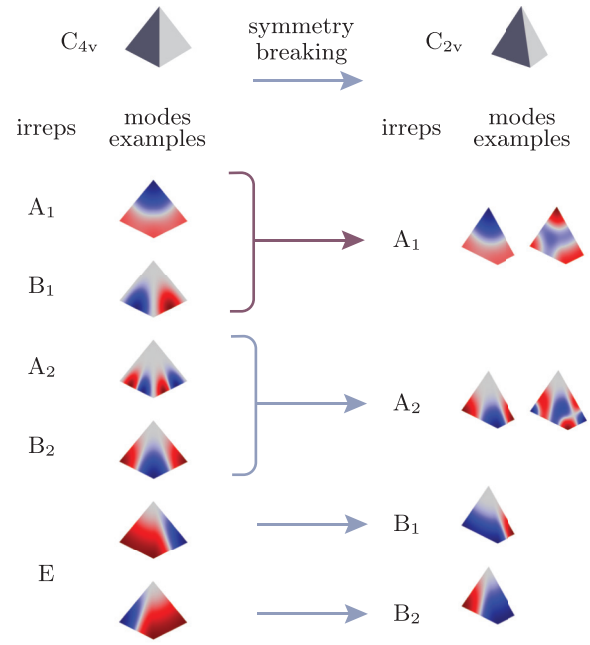

FIG. 5. Tables of irreducible representations of symmetry groups C_{4v} and C_{2v}. Examples of modes transformed under particular irreducible representations are given. The arrows show how the irreducible representations of the two groups are related to each other.

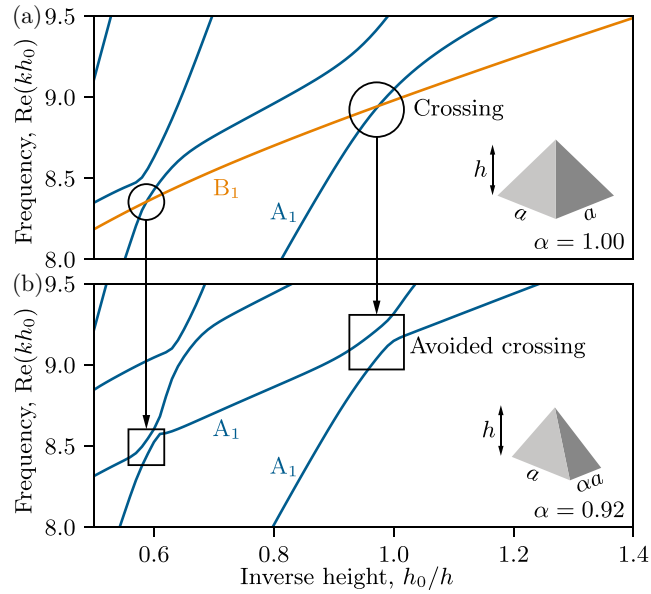

FIG. 6. Real parts of scaled with h_0 eigenvalues k of a square right pyramid ($\alpha = 1$) and a rectangular right pyramid ($\alpha = 0.92$) versus h_0/h. The branches of the square pyramid modes have different colors according to their irreps. Intersections of modes that transform under different irreps are circled. The corresponding avoided crossings are marked by a square. Geometry parameters used are $h_0 = 1$ m are $a = 1$ m.

TABLE I. Model parameters for different α values and their corresponding fitting relative errors.

α	ξ	γ	κ	Max rel. error, %
1.000	1	1	0	0.0044
0.902	$0.993783 + i0.000728$	$1.000755 - i0.001037$	$0.017148 - i0.001479$	0.0534
0.890	$0.992245 + i0.000903$	$1.000909 - i0.001272$	$0.019272 - i0.001574$	0.0113

are approximated as

$$\omega_1(h_0/h) = (2.224\,724 - i0.023\,396)\cdot h_0/h + 6.846\,411 - i0.242\,355$$

and

$$\omega_2(h_0/h) = (6.302\,923 - i0.221\,363)\cdot h_0/h + 0.606\,508 - i0.311\,79.$$

The results of fitting for each α value are presented in Table I. We choose model parameters for which there is a sufficiently accurate match with the numerical experiment. The validity of the obtained parameters extends to a wider range of heights h_0/h as long as the two-mode approximation, linear dependence of $\omega_{1,2}$, and constancy of model parameters are valid.

APPENDIX D: NUMERICAL MODELING

All simulations were performed using the Pressure Acoustics branch of the Acoustics module of the COMSOL MULTIPHYSICS software. The simulation domain was a sphere made of media material with the resonator inside. When calculating eigenmodes for Fig. 4, the perfectly matched layer (PML) was used to simulate open boundary conditions (the Sommerfeld radiation condition) on the surface of the spherical domain. To calculate eigenmodes for Figs. 3 and 6 the radiation boundary condition for a spherical wave was used instead of the PML in order to speed up calculations. All numerical modes (also termed as PML modes) were removed during postprocessing [62,63].

[1] S. A. Cummer, J. Christensen, and A. Alù, Controlling sound with acoustic metamaterials, Nat. Rev. Mater. **1**, 16001 (2016).
[2] L. Fok, M. Ambati, and X. Zhang, Acoustic metamaterials, MRS Bull. **33**, 931 (2008).
[3] G. Ma and P. Sheng, Acoustic metamaterials: From local resonances to broad horizons, Sci. Adv. **2**, e1501595 (2016).
[4] I. D. Toftul, K. Y. Bliokh, M. I. Petrov, and F. Nori, Acoustic radiation force and torque on small particles as measures of the canonical momentum and spin densities, Phys. Rev. Lett. **123**, 183901 (2019).
[5] C. Shi, R. Zhao, Y. Long, S. Yang, Y. Wang, H. Chen, J. Ren, and X. Zhang, Observation of acoustic spin, Natl. Sci. Rev. **6**, 707 (2019).
[6] S. Sepehrirahnama, S. Oberst, Y. K. Chiang, and D. A. Powell, Willis coupling-induced acoustic radiation force and torque reversal, Phys. Rev. Lett. **129**, 174501 (2022).
[7] T. Kato, *Perturbation Theory for Linear Operators* (Springer, Berlin, 1966).
[8] W. D. Heiss, The physics of exceptional points, J. Phys. A: Math. Theor. **45**, 444016 (2012).
[9] R. Schäfer, J. C. Budich, and D. J. Luitz, Symmetry protected exceptional points of interacting fermions, Phys. Rev. Res. **4**, 033181 (2022).
[10] N. Moiseyev, *Non-Hermitian Quantum Mechanics* (Cambridge University Press, Cambridge, England, 2011).
[11] J. Wiersig, Review of exceptional point-based sensors, Photon. Res. **8**, 1457 (2020).
[12] J.-H. Park, A. Ndao, W. Cai, L. Hsu, A. Kodigala, T. Lepetit, Y.-H. Lo, and B. Kanté, Symmetry-breaking-induced plasmonic exceptional points and nanoscale sensing, Nat. Phys. **16**, 462 (2020).
[13] M.-A. Miri and A. Alù, Exceptional points in optics and photonics, Science **363**, eaar7709 (2019).
[14] R. El-Ganainy, K. G. Makris, M. Khajavikhan, Z. H. Musslimani, S. Rotter, and D. N. Christodoulides, Non-Hermitian physics and PT symmetry, Nat. Phys. **14**, 11 (2018).
[15] L. Feng, R. El-Ganainy, and L. Ge, Non-Hermitian photonics based on parity–time symmetry, Nat. Photon. **11**, 752 (2017).
[16] W. Tang, X. Jiang, K. Ding, Y.-X. Xiao, Z.-Q. Zhang, C. T. Chan, and G. Ma, Exceptional nexus with a hybrid topological invariant, Science **370**, 1077 (2020).
[17] A. Li, H. Wei, M. Cotrufo, W. Chen, S. Mann, X. Ni, B. Xu, J. Chen, J. Wang, S. Fan, C.-W. Qiu, A. Alù, and L. Chen, Exceptional points and non-Hermitian photonics at the nanoscale, Nat. Nanotechnol. **18**, 706 (2023).
[18] J. Schindler, A. Li, M. C. Zheng, F. M. Ellis, and T. Kottos, Experimental study of active LRC circuits with $\mathcal{PT}$ symmetries, Phys. Rev. A **84**, 040101(R) (2011).
[19] V. Achilleos, G. Theocharis, O. Richoux, and V. Pagneux, Non-Hermitian acoustic metamaterials: Role of exceptional points in sound absorption, Phys. Rev. B **95**, 144303 (2017).
[20] R. Fleury, D. Sounas, and A. Alù, An invisible acoustic sensor based on parity-time symmetry, Nat. Commun. **6**, 5905 (2015).
[21] B. Midya, H. Zhao, and L. Feng, Non-Hermitian photonics promises exceptional topology of light, Nat. Commun. **9**, 2674 (2018).
[22] M. Pan, H. Zhao, P. Miao, S. Longhi, and L. Feng, Photonic zero mode in a non-Hermitian photonic lattice, Nat. Commun. **9**, 1308 (2018).
[23] A. Canós Valero, V. Bobrovs, T. Weiss, L. Gao, A. S. Shalin, and Y. Kivshar, Bianisotropic exceptional points in an isolated dielectric nanoparticle, Phys. Rev. Res. **6**, 013053 (2024).
[24] A. Canós Valero, H. K. Shamkhi, A. S. Kupriianov, T. Weiss, A. A. Pavlov, D. Redka, V. Bobrovs, Y. Kivshar, and A. S. Shalin, Superscattering emerging from the physics of bound states in the continuum, Nat. Commun. **14**, 4689 (2023).

[25] H. Cao and J. Wiersig, Dielectric microcavities: Model systems for wave chaos and non-Hermitian physics, Rev. Mod. Phys. **87**, 61 (2015).
[26] M. Tsimokha, V. Igoshin, A. Nikitina, I. Toftul, K. Frizyuk, and M. Petrov, Acoustic resonators: Symmetry classification and multipolar content of the eigenmodes, Phys. Rev. B **105**, 165311 (2022).
[27] S. Gladyshev, K. Frizyuk, and A. Bogdanov, Symmetry analysis and multipole classification of eigenmodes in electromagnetic resonators for engineering their optical properties, Phys. Rev. B **102**, 075103 (2020).
[28] Z. Sadrieva, K. Frizyuk, M. Petrov, Y. Kivshar, and A. Bogdanov, Multipolar origin of bound states in the continuum, Phys. Rev. B **100**, 115303 (2019).
[29] S. Guenneau, A. Movchan, G. Pétursson, and S. A. Ramakrishna, Acoustic metamaterials for sound focusing and confinement, New J. Phys. **9**, 399 (2007).
[30] M. Eichenfield, J. Chan, R. M. Camacho, K. J. Vahala, and O. Painter, Optomechanical crystals, Nature (London) **462**, 78 (2009).
[31] M. Nirschl, A. Blüher, C. Erler, B. Katzschner, I. Vikholm-Lundin, S. Auer, J. Vörös, W. Pompe, M. Schreiter, and M. Mertig, Film bulk acoustic resonators for DNA and protein detection and investigation of in vitro bacterial S-layer formation, Sens. Actuat. A **156**, 180 (2009).
[32] S. Thomas, M. Cole, F. H. Villa-López, and J. W. Gardner, High frequency surface acoustic wave resonator-based sensor for particulate matter detection, Sens. Actuat. A **244**, 138 (2016).
[33] T. Lee, T. Nomura, X. Su, and H. Iizuka, Fano-like acoustic resonance for subwavelength directional sensing: 0–360 degree measurement, Adv. Sci. **7**, 1903101 (2020).
[34] M. Molerón and C. Daraio, Acoustic metamaterial for subwavelength edge detection, Nat. Commun. **6**, 8037 (2015).
[35] M. Krasikova, S. Krasikov, A. Melnikov, Y. Baloshin, S. Marburg, D. A. Powell, and A. Bogdanov, Metahouse: Noise-insulating chamber based on periodic structures, Adv. Mater. Technol. **8**, 2200711 (2023).
[36] Muhammad and C. W. Lim, From photonic crystals to seismic metamaterials: A review via phononic crystals and acoustic metamaterials, Arch. Comput. Methods Eng. **29**, 1137 (2022).
[37] A. Gupta, R. Sharma, A. Thakur, and P. Gulia, Metamaterial foundation for seismic wave attenuation for low and wide frequency band, Sci. Rep. **13**, 2293 (2023).
[38] L. D. Landau and E. M. Lifshitz, *Fluid Mechanics* (Pergamon Press, Oxford, England, 1987).
[39] S. Solimeno, B. Crosignani, and P. DiPorto, *Guiding, Diffraction, and Confinement of Optical Radiation* (Academic Press, San Diego, 1986).
[40] A. Sommerfeld, Die Greensche funktion der schwingungslgleichung, Jahresber. Deutsch. Math.-Verein. **21**, 309 (1912).
[41] A. V. Shubnikov, On the works of Pierre Curie on symmetry, Comput. Math. Appl. **16**, 357 (1988).
[42] M. Petrashen, E. Trifonov, S. Chomet, and J. Martin, *Applications of Group Theory in Quantum Mechanics*, Dover Books on Physics (Dover, New York, 2009).
[43] E. A. Muljarov and T. Weiss, Resonant-state expansion for open optical systems: generalization to magnetic, chiral, and bi-anisotropic materials, Opt. Lett. **43**, 1978 (2018).
[44] I. Deriy, I. Toftul, M. Petrov, and A. Bogdanov, Bound states in the continuum in compact acoustic resonators, Phys. Rev. Lett. **128**, 084301 (2022).
[45] A. Zee, *Group Theory in a Nutshell for Physicists* (Princeton University Press, Princeton, NJ, 2016).
[46] L. D. Landau and E. M. Lifshitz, *Quantum Mechanics* (Pergamon Press, Oxford, England, 1977).
[47] J. Lasa-Alonso, C. Devescovi, C. Maciel-Escudero, A. García-Etxarri, and G. Molina-Terriza, On the origin of the Kerker phenomena, arXiv:2306.12762.
[48] M. Hamidi, K. Koshelev, S. Gladyshev, A. C. Valero, M. Hentschel, H. Giessen, Y. Kivshar, and T. Weiss, Quasi-Babinet principle in dielectric resonators and Mie voids, arXiv:2312.04082.
[49] Y. Cheng, C. Zhou, B. G. Yuan, D. J. Wu, Q. Wei, and X. J. Liu, Ultra-sparse metasurface for high reflection of low-frequency sound based on artificial Mie resonances, Nat. Mater. **14**, 1013 (2015).
[50] Z. Liang and J. Li, Extreme acoustic metamaterial by coiling up space, Phys. Rev. Lett. **108**, 114301 (2012).
[51] A. Melnikov, Y. K. Chiang, L. Quan, S. Oberst, A. Alù, S. Marburg, and D. Powell, Acoustic meta-atom with experimentally verified maximum Willis coupling, Nat. Commun. **10**, 3148 (2019).
[52] L. D. Landau and E. M. Lifshitz, *Quantum Mechanics* (Pergamon Press, Oxford, England, 1977).
[53] Character table for point group D∞h, 2021 [Online; accessed 21 Mar. 2021].
[54] Non-Crystallographic: Dinfh (2001) [Online; accessed 21 Mar, 2021].
[55] L. Quan, Y. Ra'di, D. L. Sounas, and A. Alù, Maximum Willis coupling in acoustic scatterers, Phys. Rev. Lett. **120**, 254301 (2018).
[56] C. F. Sieck, A. Alù, and M. R. Haberman, Origins of Willis coupling and acoustic bianisotropy in acoustic metamaterials through source-driven homogenization, Phys. Rev. B **96**, 104303 (2017).
[57] J. R. Willis, The nonlocal influence of density variations in a composite, Int. J. Solids Struct. **21**, 805 (1985).
[58] J. Wiersig, Sensors operating at exceptional points: General theory, Phys. Rev. A **93**, 033809 (2016).
[59] D. N. Maksimov, A. F. Sadreev, A. A. Lyapina, and A. S. Pilipchuk, Coupled mode theory for acoustic resonators, Wave Motion **56**, 52 (2015).
[60] M. A. Miroliubov, A. K. Samusev, I. D. Toftul, and M. I. Petrov, Spectral characteristics and time dynamics of tunable acoustic resonators in the strong coupling regime, JETP Lett. **113**, 547 (2021).
[61] M. B. Doost, W. Langbein, and E. A. Muljarov, Resonant-state expansion applied to three-dimensional open optical systems, Phys. Rev. A **90**, 013834 (2014).
[62] C. Sauvan, T. Wu, R. Zarouf, E. A. Muljarov, and P. Lalanne, Normalization, orthogonality, and completeness of quasinormal modes of open systems: the case of electromagnetism [Invited], Opt. Express **30**, 6846 (2022).
[63] W. Yan, R. Faggiani, and P. Lalanne, Rigorous modal analysis of plasmonic nanoresonators, Phys. Rev. B **97**, 205422 (2018).
[64] A. A. Bogdanov, K. L. Koshelev, P. V. Kapitanova, M. V. Rybin, S. A. Gladyshev, Z. F. Sadrieva, K. B. Samusev, Y. S. Kivshar,

and M. F. Limonov, Bound states in the continuum and Fano resonances in the strong mode coupling regime, Adv. Photon. **1**, 016001 (2019).

[65] J. Sólyom, Consequences of Symmetries, in *Fundamentals of the Physics of Solids: Volume I: Structure and Dynamics* (Springer, Berlin, 2007), Chap. 6, pp. 171–201.

[66] H.-Z. Chen, T. Liu, H.-Y. Luan, R.-J. Liu, X.-Y. Wang, X.-F. Zhu, Y.-B. Li, Z.-M. Gu, S.-J. Liang, H. Gao, L. Lu, L. Ge, S. Zhang, J. Zhu, and R.-M. Ma, Revealing the missing dimension at an exceptional point, Nat. Phys. **16**, 571 (2020).

[67] C. M. Jiang, J. Huang, A. Tagliasacchi, and L. Guibas, ShapeFlow: learnable deformations among 3D shapes, in *NIPS'20: Proceedings of the 34th International Conference on Neural Information Processing Systems* (Curran Associates, Red Hook, NY, 2020), pp. 9745–9757.

[68] Transform sphere into a cube (2024) [Online; accessed 10 Feb, 2024].

[69] A. Hatcher, *Algebraic Topology* (Cambridge University Press, Cambridge, England 2002).

[70] L. P. Bouckaert, R. Smoluchowski, and E. Wigner, Theory of Brillouin zones and symmetry properties of wave functions in crystals, Phys. Rev. **50**, 58 (1936).

[71] H. A. Bethe, Splitting of terms in crystals, in *Selected Works of Hans A. Bethe* (World Scientific, Singapore, 1997), Vol. 18, pp. 1–72.

[72] D. L. Rousseau, R. P. Bauman, and S. P. S. Porto, Normal mode determination in crystals, J. Raman Spectrosc. **10**, 253 (1981).